International Journal of Geology, Agriculture and Environmental Sciences
Volume – 3 Issue – 6 December 2015
Website: www.woarjournals.org/IJGAES *ISSN: 2348-0254*

Fluvial Sediment Transport in a Forested Catchment Influenced by Slope Failure

Md. Motaleb Hossain[1], Kazuhisa A. Chikita[*2], Yoshitaka Sakata[2], Takuto Miyamoto[1]

[1]Graduate School of Science, Hokkaido University,
Sapporo, 060-0810, Japan

[2]Department of Earth and Planetary Sciences, Faculty of Science, Hokkaido University,
Sapporo, 060-0810, Japan

**Corresponding author (Professor and PhD)*

Abstract: *In order to clarify how fluvial sediment behaves in a forested catchment accompanied by slope failure, hourly time series of suspended sediment concentration C (mg L^{-1}), discharge Q (m^3 s^{-1}) and suspended sediment load L (g s^{-1}) (= C·Q) of river were obtained in the forested (88.3 % of 62.46 km^2 in area) Oikamanai River catchment, Hokkaido, Japan. Catchment geology is early Miocene to Pliocene sedimentary bedrock, accompanied by currently active faults, and forest-slope soils contain two permeable sandy tephra layers, Tarumae Ta-b (1667) at ca. 40 cm depth and Shikotsu Spfa-1 (ca. 40000 yr ago) at more depth. The geology and tephra layers tend to frequently produce slope failure such as landslide and bank collapse under rainfall. River runoff events with maximum Q >2.0 m^3 s^{-1} were recorded 28 times in the rainfall season (April to November) of 2011 - 2012, of which ten runoff events received the extra sediment supply from slope failure. Relations between diurnal sediment yield (g m^{-2} d^{-1}) and diurnal runoff rate (mm d^{-1}) during each event period were explored for all the events. As a result, the runoff events with slope failure exhibited the sediment yield 2.2 times as high as that for the runoff events without slope failure. Total sediment yield (g m^{-2}) for all the events in 2012 was 2.6 times as large as that in 2011. This is due to high sediment yield (157.6 g m^{-2}) in the largest runoff event (total rainfall 221.0 mm per 47 h) in early May 2012, accompanied by slope failure.*

Keywords: sediment load, slope failure, sediment yield, runoff rate

1. Introduction

It is important to know how sediment is yielded and fluvially loaded in a catchment with respect to the forest and land managements on small time scale of one to 100 years order and the landform development on large time scale of 10^3 to 10^5 years [1]. The acquirement of discharge and suspended sediment concentration time series in a river allow us to explore the source location, availability and loading processes of sediment in the catchment [2][3], and to simulate long-term sediment yield or sediment load by modelling [4][5]. Dynamic processes of slope failure such as landslide in the catchment have been investigated by many geologists, geomorphologists and geophysists [6][7][8]. However, studies on subsequent fluvial sedimentation processes, connected to sediment load of river, are not enough [9].

There are many models of sediment yield and sediment load in a catchment such as USLE (the Universal Soil Loss Equation), MUSLE (modified USLE) in SWAT (Soil and Water Assessment Tool), etc.[10][11][12]. However, how subsurface flow or surface flow on hillslope in a forested catchment erodes soils and transports them in suspension to river channels is not yet known in detail.

In this paper, how river-suspended sediment load is influenced by slope failure such as landslide and bank collapse is explored from hourly time series of discharge, suspended sediment concentration (SSC) and sediment load of river.

2. Study area and methods

2.1 Study area

The Oikamanai River is a main influent river of the Oikamanai Lagoon in the Tokachi coastal region of southeastern Hokkaido, Japan (Fig. 1)[13]. The river catchment (42°33'46" to 42°40'40"N, 143°21'47" to 143°28'36"E; altitude, 6 m to 330 m asl) upstream of site R1 has the area of 62.46 km2, the mean slope angle of 17° and the mean riverbed gradient of 0.033 (Fig. 1)[14]. The digital elevation model (DEM) in Figure 1 is made up by 0.1 km × 0.1 km mesh. The distribution of slope angle corresponds to that of the surface geology (Fig. 2); the upper, middle and lower regions with relatively steep slope in the northwest to southeast directions are occupied by sedimentary rocks of early to middle Miocene, middle to late Miocene and late Miocene to Pliocene, respectively, and the lowest region with relatively gentle slope just upstream of site R1 by alluvial flood deposits [15]. The sedimentary rocks are composed of conglomerate, sandstone, mudstone, siltstone and tuff. The sedimentary rocks in the mountainous regions are accompanied by many faults, which are due to the orogenic movement of the Hidaka Range at ca. 45 km southwest of the catchment. Of all bedrocks in Japan, the Neogene sedimentary rocks tend to most frequently produce land slide under heavy rainfall [16]. Sandy pyroclastic deposits (Shikotsu, Spfa-1) of Late Pleistocene (40000 yr ago) are distributed along the border of flood plain and forest regions. The Spfa-1 tephra broadly covers the bedrocks in the forest, and relatively new tephra, Tarumae Ta-b in 1667 is

located at ca. 40 cm depth of forest soil [15]. These tephra layers on catchment slope tend to produce surface collapse by heavy rainfall or snowmelt.

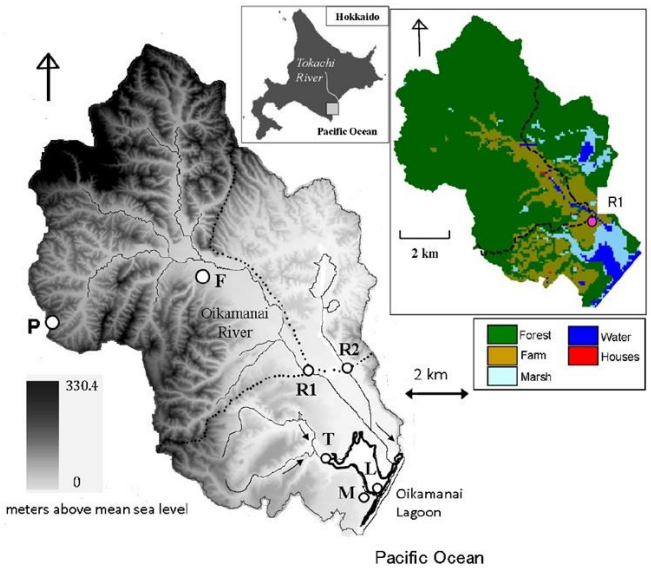

Figure 1: Location of the Oikomanai River catchment in Hokkaido, Japan, and observation sites in the catchment, shown by the digital elevation model (DEM). The land use map is also shown (right) [14]

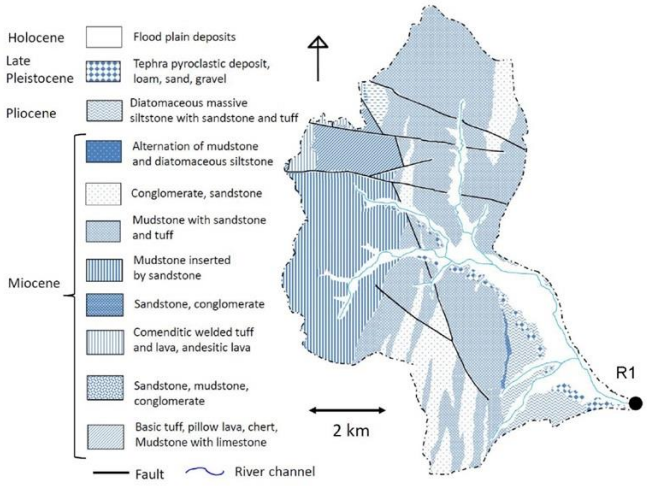

Figure 2: Geology of the catchment upstream of site R1 [14]

The catchment upstream of site R1 is covered by 88.3 % forest in the mountainous region, 10.6 % farmland (mostly, grassland) on the lowest alluvial plain and others (Fig. 1). The forest is composed of ca. 50% broad-leaved and ca. 50% coniferous (mainly, Sakhalin fir; *Abies sachalinensis*) trees.

2.2 Methods

The monitoring of water level, air temperature, water temperature and water turbidity at site R1 was performed at 1 hour intervals by HOBO air pressure and water pressure loggers with temperature sensors (Onset Computer, Inc., USA; the range of 69 – 207 kPa and the accuracy of ±0.62 kPa for pressure, and the range of -20 to 50 °C and the accuracy of ±0.2 °C for temperature), and a self-recording turbidimeter of infrared back-scattering type with a window-cleaning wiper (type ATU3-8M, Advantec, Inc., Japan, with a range of 0 - 20000 ppm and an accuracy of ±20 ppm), respectively, in April 2011 to November 2012. Instantaneous turbidity (ppm) was measured ten times at 1 sec interval every 1 hour signal and averaged for the 10 samplings. The averaged turbidity was converted into suspended sediment concentration (SSC; mg L^{-1}) from simultaneous water samplings by a depth-integrating sampler (Fig. 3). Two regression lines with a boundary at 200 ppm were acquired, since relations between electric signal and turbidity are obtained at 0 – 200 ppm and 200 – 20,000 ppm in manufacture, using suspension of kaolin powder.

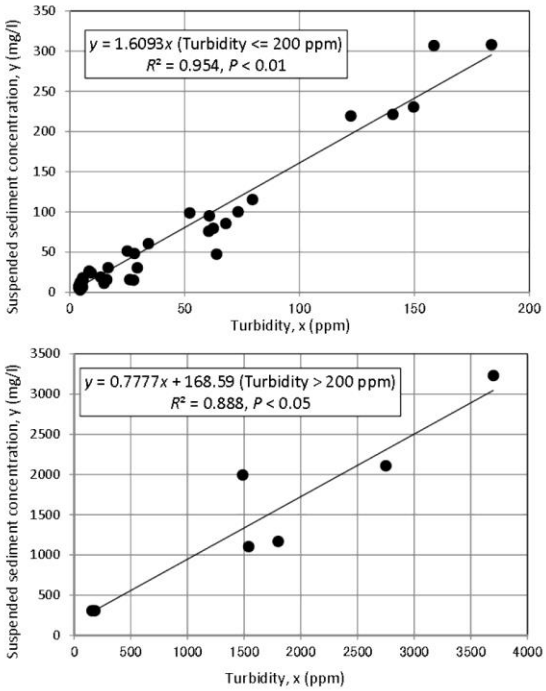

Figure 3: Relationships between water turbidity (ppm) and suspended sediment concentration (SSC: mg/L), separated by 200 ppm turbidity

Water level, h (m), at site R1 was changed into river discharge, Q (m^3 s^{-1}), by an h - Q rating curve, $Q=7.740\cdot(h+0.1507)^2$ (R^2 = 0.935, p < 0.01), which was obtained by measuring discharge several times per year and, at h > 0.5 m, applying the Manning equation to the channel cross-section at site R1 on assumption of constant Manning roughness coefficient at any water level. The route of the Oikamanai River channel is artificially regulated by concrete blocks constructed in 1996. The sediment load, L (g s^{-1}), was calculated by $L = C \times Q$, where C is suspended sediment concentration (mg L^{-1}).

The weather data were obtained at site M (rainfall and air temperature) near the Oikamanai Lagoon [13] at 4.0 km south-southeast of site R1, and at two weather stations at the Taiki Aerospace Research Field (rainfall, air temperature, solar radiation, and wind speed and direction) 9.6 km south of site R1 and Taiki town (snow depth, rainfall, air temperature, and wind speed and direction) 18.9 km southwest of site R1. The distinction between rainfall and snowfall in the catchment was performed under air temperature more than 0 °C at site M (altitude, 6 m asl).

3. Observational Results and Discussion

Figure 4 shows hourly time series of discharge, suspended sediment concentration (SSC), suspended sediment load and water temperature at site R1, air temperature and precipitation at the Aerospace Research Field, and snow depth at Taiki town in April 2011 to March 2013. As shown by water temperature at ca. 0 °C, the Oikamanai River was frozen down to the depth of the pressure logger for 6 December 2011 to 30 March 2012, and 18 December 2012 to 19 March 2013. The rating curve of $Q=7.740\cdot(h+0.1507)^2$ was then not applicable at site R1, because the covered-ice growth and snow accumulation on the ice substantially increase the water pressure recorded. As a result, the accurate observation of snowmelt runoffs in the snowmelt season was difficult, because snowmelt water then flew on the covered ice. Hence, only rainfall river runoff events under ice- or snow-free condition of the catchment are here discussed.

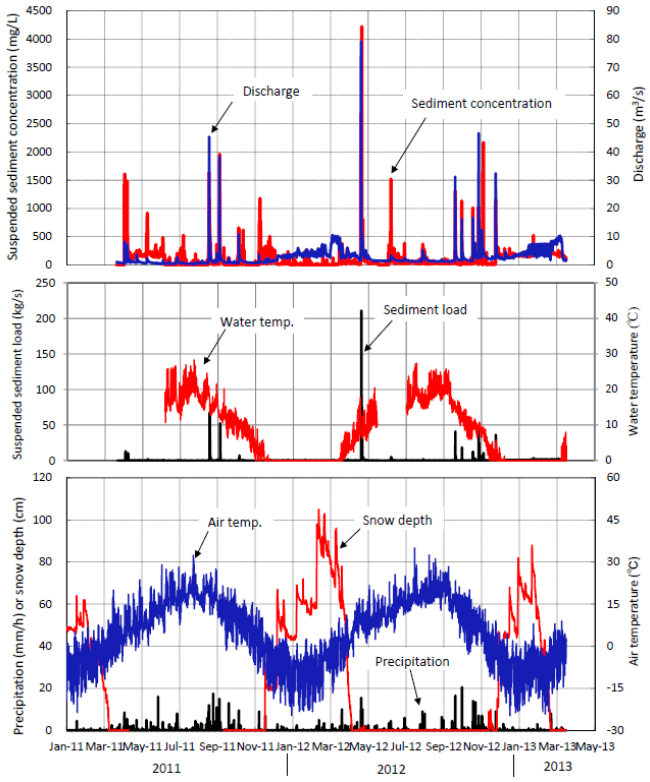

Figure 4: Hourly time series of discharge and water temperature at site R1, air temperature and precipitation at the Taiki Aerospace Research Field, and snow depth at Taiki town

Rainfall runoff events with maximum discharge of more than 2.0 $m^3\ s^{-1}$ were observed 28 times at site R1 in April to November of 2011 and 2012 (Table 1). The duration, *D* (h), of runoff events were defined as time periods when both discharge and SSC start to increase and SSC reaches to a final point of abrupt decrease after maximum discharge and SSC. The largest runoff event (no. 13 in Table 1) occurred by a heavy rainfall (totally, 221 mm; Figure 4). The peak discharge was 79.0 $m^3\ s^{-1}$ at 1400 h on 4 May 2012, accompanied by SSC at 2,670 mg L^{-1}. However, the highest SSC at 4,220 mg L^{-1} was recorded at 2300 h on 5 May 2012 during declining discharge (7.4 $m^3\ s^{-1}$) after rainfall (Fig. 5). This suggests that the extra sediment supply to the channel reach upstream of site R1 occurred by riverbank collapse or landslide on the surrounding slope. Of all the runoff events, ten runoff events (Event no. 1, 2, 4, 7, 9, 12, 13, 18, 24 and 26 in Table 1) exhibited a great fluctuation in SSC after maximum discharge or corresponding maximum SSC. Runoff events with slope failure tend to more frequently occur in spring (April – May) and autumn (late September –November). This suggests that the summer growth of understory in forest and vegetation on riparian slope prevents slope failure.

Table 1: River runoff events with maximum discharge of more than 2 $m^3\ s^{-1}$ observed in 2011 – 2012. *Q*: Discharge *S*: Suspended sediment concentration *L*: Suspended sediment load

No.	Time period of runoff event	Duration (h)	Mean *Q* (m^3/s)	Max *Q* (m^3/s)	Mean *S* (mg/L)	Max *S* (mg/L)	Mean *L* (kg/s)	Max *L* (kg/s)	Total rainfall (mm)	Remark
2011										
1	0000 h, 24 April - 0200 h, 25 Ap	26	7.69	14.0	957	1610	6.7	13.1	71.5	with failure
2	0800 h, 28 April - 2300 h, 28 Ap	15	5.65	7.10	645	1480	3.8	10.4	47.0	with failure
3	1400 h, 13 May - 0100 h, 14 Ma	11	3.04	3.53	225	253	0.69	0.88	37.0	
4*	0200 h, 29 May - 0100 h, 31 Ma	47	1.84	2.34	492	915	0.97	1.86	40.5	with failure
5	2100 h, 16 July - 0000 h, 18 July	27	2.02	2.71	77.5	205	0.18	0.56	32.5	
6	2300 h, 4 Sep. - 1000 h, 5 Sep.	11	1.85	2.54	118	228	0.24	0.55	18.0	
7	1300 h, 5 Sep. - 0900 h, 8 Sep.	68	10.90	45.3	611	1640	10.3	68.2	21.0	with failure
8	2000 h, 17 Sep. - 1300 h, 20 Sep	65	2.55	4.07	74.5	364	0.23	1.44	42.5	
9	0000 h, 22 Sep. - 0800 h, 23 Sep	32	12.9	38.3	817	1960	13.9	52.5	88.0	with failure
10	0100 h, 24 Sep. - 0900 h, 24 Sep	8	3.09	3.29	106	112	0.33	0.37	12.0	
11	2100 h, 22 Oct. - 1500 h, 23 Oct.	18	6.38	10.9	368	656	2.7	7.1	59.5	
12	0500 h, 24 Nov. - 1800 h, 26 Nov	61	1.47	3.65	465	1180	0.62	1.4	24.0	with failure
2012										
13	0300 h, 4 May - 0200 h, 6 May	47	33.3	79.0	1690	4220	58.2	211	221.0	with failure
14	1500 h, 6 May - 2200 h, 7 May	31	6.62	9.69	362	810	2.5	5.3	30.5	
15	1800 h, 11 May - 0300 h, 13 Ma	33	4.30	5.17	128	209	0.57	1.1	32.0	
16	1900 h, 15 May - 0700 h, 17 Ma	36	2.88	3.42	41.6	65.4	0.12	0.22	19.5	
17	1500 h, 20 June - 0100 h, 22 Jun	34	2.86	3.40	463	1520	1.4	5.1	48.5	
18	0100 h, 10 Aug. - 1800 h, 12 Au	65	3.33	5.20	151	368	0.56	1.8	44.5	with failure
19	1500 h, 13 Aug. - 1100 h, 14 Au	20	2.77	3.42	37.5	61.4	0.11	0.19	17.0	
20	0400 h, 1 Oct. - 0200 h, 2 Oct.	22	11.7	31.2	499	1310	8.0	40.9	89.5	
21	1900 h, 11 Oct. - 1600 h, 12 Oct.	21	6.63	16.3	415	1130	3.7	18.4	40.0	
22	0600 h, 29 Oct. - 2000 h, 29 Oct.	14	9.34	16.7	421	1010	4.7	12.5	53.0	
23	2300 h, 1 Nov. - 1700 h, 3 Nov.	42	5.05	7.75	157	382	0.86	2.7	42.0	
24	0900 h, 7 Nov. - 1800 h, 8 Nov.	33	22.1	46.7	693	1030	17.6	43.0	77.0	with failure
25	1400 h, 12 Nov. - 1300 h, 13 Nov	23	8.20	12.5	291	583	2.7	7.3	36.5	
26	1000 h, 14 Nov. - 1300 h, 15 Nov	27	5.32	5.83	643	2167	3.4	10.7	16.5	with failure
27	2200 h, 28 Nov. - 2000 h, 29 Nov	22	2.70	3.00	21.5	46.6	0.06	0.13	9.5	
28	1400 h, 4 Dec. - 0500 h, 6 Dec.	39	14.5	32.4	560	1150	10.2	36.2	75.5	

* including continual two runoff events

Figure 5 shows time series of hourly rainfall, discharge, SSC and sediment load for events of (a) no. 1, (b) no. 4, (c) no. 12 and (d) no. 13, accompanied by the extra sediment supply. There are two types for the extra sediment supply; (1) SSC increases until maximum discharge appears, but subsequently higher SSC continues for more than half a day (Figure 5b, 5c and 5d). (2) SSC is peaked at or around maximum discharge and then greatly fluctuates within about half a day (Figure 5a). In nos. 4 and 12 events (Figure 5b and 5c), the temporal variation of sediment load after maximum discharge is influenced by SSC rather than discharge, since discharge is then relatively stable on declining limb.

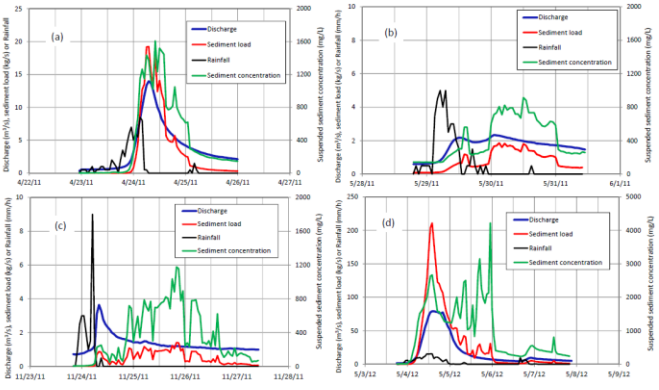

Figure 5: Hourly time series of discharge, SSC and sediment load at site R1, and rainfall at site P for river runoff events with slope failure. (a) no. 1, (b) no. 4, (c) no. 12 and (d) no. 13 in Table 1

Examples of runoff events without extra sediment supply (nos. 6-9 events in Table 1) are shown in Figure 6. The SSC

then varied in phase with discharge. There is a time difference of 0 – 2 h between peak discharge and peak SSC. The bank collapse and landslide could be induced from gravitational instability of bank sediment and surrounding slope soil with increasing water storage during rainfall, respectively. In Figure 5, it should be noted that the extra sediment supply to the river channel occurred by such surface failure after rainfall.

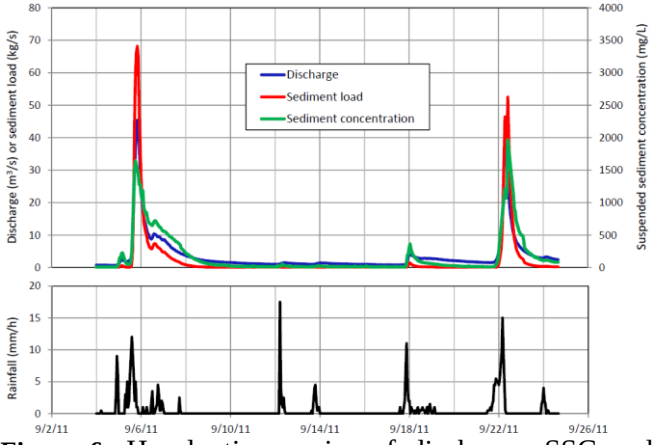

Figure 6: Hourly time series of discharge, SSC and sediment load at site R1, and rainfall at site P for river runoff events without slope failure

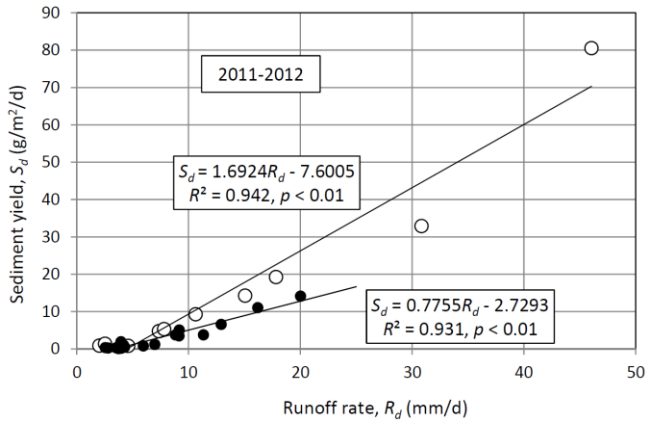

Figure 7: Relations between diurnal runoff rate R_d (mm d^{-1}) and diurnal sediment yield S_d (g m^{-2} d^{-1}) for rainfall runoff events with slope failure (white circles) and without slope failure (black circles)

Figure 7 shows relations between diurnal runoff rate R_d (mm d^{-1}) and diurnal sediment yield S_d (g m^2 d^{-1}) for all the runoff events. R_d and S_d were calculated as $R_d = 24{\cdot}1000{\cdot}R{\cdot}D^{-1}{\cdot}A^{-1}$ and $S_d = 24{\cdot}1000{\cdot}S{\cdot}D^{-1}{\cdot}A^{-1}$, where R is total discharge (m^3) for the event duration D (h), A is catchment area (m^2) and S is total sediment load (g) for D. Though there are only ten plots for runoff events with slope failure (white circles in Fig. 7), they seem to exhibit sediment yield 2.2 times as high as that for the events without slope failure (black circles in Fig. 7), as shown by the magnitude of the slope for the two regression lines. At R_d < ca. 10 mm d^{-1}, however, the $R_d - S_d$ relations are almost same. This indicates that, with or without slope failure, temporal variations of discharge and sediment load in small runoff events are similar. The linear relationship for the events without slope failure (white circles in Fig. 7) suggests that the intensity of effective rainfall proportionally increases the amount of sediment eroded and transported by surface flow or subsurface flow on the catchment slope and riparian slope. The other linear relationship for events with slope failure means that, being proportional to the magnitude of effective rainfall, the amount of sediment supplied by slope failure is added. Total sediment yield (g m^{-2}) for all the events in April – November 2012 was 2.6 times as large as that in April – November 2011, although the number of runoff events with slope failure is smaller in 2012 (Table 1). This is due to high sediment yield (157.6 g m^{-2}) in the largest runoff event (total rainfall 221.0 mm per 47 h) in early May 2012, accompanied by slope failure (Fig. 5d).

4. Conclusion

The acquirement of hourly discharge, SSC and sediment load time series allowed us to detail the condition of fluvial sediment transport from slope failure in the catchment upstream of the observation site. However, in order to predict seasonal change of sediment yield in a forested catchment, the hydrological slope survey and modelling at an hourly base considering the slope instability from rainfall are needed.

References

[1] V. R. Baker, "Regional Landforms Analysis" in "Geomorphology from Space: A Global Overview of Regional Landforms", N. M. Short and R. W. Blair, Jr. (eds), Geocarto International, 2, 718pp, 1987.

[2] D. E. Walling and B. W. Webb, "Sediment Availability and the Prediction of Storm-Period Sediment Yields,", IAHS Publ. No. 137, pp. 327-337, 1982.

[3] N. E. M. Asselman, "Suspended Sediment Dynamics in a Large Drainage Basin: the River Rhine. Hydrological Processes, 13, pp. 1437-1450, 1999.

[4] M. C. McCullough, D. E. Eisenhauer and M. Dosskey, "Modeling Runoff and Sediment Yield from a Terraced Watershed Using WEPP. USDA Forest Service/UNL Faculty Publications, Paper No. MC08-118, 12pp, University of Nebraska Lincoln, 2008.

[5] I. Qiu, F. Zheng, R. Yin, "SWAT-Based Runoff and Sediment Simulation in a Small Watershed, the Loessial Hilly-Gullied Region of China: Capabilities and Challenges", International Journal of Sediment Research 27, pp. 226-234, 2012.

[6] F. Ashland and G. N. McDonald, "Geologic Characteristics and Movement of the Meadow Creek Landslide, part of the Coal Hill Landslide Complex, Western Kane County, Utah", in "Geology of South-Central Utah", S. M. Camey, D. E. Tabet and C. L. Johnson (eds), Utah Geological Association Publication, 39, pp. 38-60, 2010.

[7] G. Ekstrom and C. P. Stark, "Simple Scaling of Catastrophic Landslide Dynamics", Science, 339, pp. 1416-1419, 2013.

[8] J. L. Zˆezere, R. M. Trigo and I. F. Trigo, "Shallow and Deep Landslides Induced by Rainfall in the Lisbon Region (Portugal): Assessment of Relationships with the North Atlantic Oscillation", Natural Hazards and Earth System Sciences, 5, pp. 331–344, 2005.

[9] Z.-X. Tsai, G. J.-Y. You, H.-Y. Lee1 and Y.-J. Chiu, "Modeling the Sediment Yield from Landslides in the Shihmen Reservoir Watershed, Taiwan", Earth Surf. Process. Landforms, 38, pp. 661–674, 2013.

[10] W. S. Merritt, R. A. Letcher and A. J. Jakeman, "A Review of Erosion and Sediment Transport Models. Environmental Modelling & Software, 18, pp. 761–799, 2003.
[11] H. Aksoyand and M. L Kavvas, "A Review of Hillslope and Watershed Scale Erosion and Sediment Transport Models", Catena, 64, pp. 247–271, 2005.
[12] M. Talebizadeh, S. Morid, S. A. Ayyoubzadeh and M. Ghasemzadeh, "Uncertainty Analysis in Sediment Load Modeling using ANN and SWAT Model", Water Resources Managements, 24, pp. 1747–1761, 2010.
[13] K. A. Chikita, W. Iwasaka, A.A. Mamun, K. Ohmori, K. and Y. Itoh, "The Role of Groundwater Outflow in the Water Cycle of a Coastal Lagoon Sporadically Opening to the Ocean. Journal of Hydrology, 464-465, pp. 423-430, 2012.
[14] M. M. Hossain, K. A. Chikita, Y. Sakata, T. Miyamoto, and Y. Ochiai, "Groundwater Leakage and River Runoff in a Catchment Influenced by Tectonic Movement", Open Journal of Modern Hydrology, 5, pp. 32-44, 2015.
[15] S. Yamaguchi, H. Sato and S. Mastui, "Geology of the Churui Region, Hokkaido", Geological Survey of Japan, National Institute of Advanced Industrial Science and Technology, 68pp., 2003.
[16] K. Araiba, T. Nozaki, B. Jeong and Y. Fukumoto, "Distribution of Landslides and their Geological Characteristics in Japan", .Journal of the Japanese Landslide Society, 44, pp. 37-44, 2008.